Conference Proceedings

EuroSun 2014
Aix-les-Bains (France), 16 – 19 September 2014

Measurement of the All Sky Spectral Radiance Distribution Using a Fisheye Camera and Principal Component Analysis

Yoshiaki Uetani

Kyoto University, Kyoto (JAPAN)

Abstract

A new method was developed to measure the spectral radiance of all sky elements using a general purpose digital camera with a circular fisheye lens. The method provides sufficient accuracy for solar energy applications such as daylighting design, photosynthesis analyses and photovoltaic evaluations. The instrument is portable for field measurements in various climates. The digital camera with the fisheye lens is colorimetrically calibrated using a xenon lamp and a spectroradiometer to obtain the calibration functions which transfer the video signal values RGB on a digital color image into the absolute values of CIE 1931 tristimulus values XYZ pixel by pixel. The calibrated fisheye digital camera measures the all sky distribution of the XYZ tristimulus values which are also useful for measuring all sky distributions of luminance and correlated color temperature. The XYZ tristimulus values are transferred into the all sky spectral radiance distribution using the eigenvectors obtained by principal component analysis of spectral radiance data of sky elements measured by a spectroradiometer under various weather conditions. The accuracy of the method is experimentally validated by comparing with the spectral radiance of sky elements measured by the spectroradiometer.

1. Introduction

Most solar energy applications have been designed based on irradiance [W m^{-2}] and radiance [W m^{-2} sr^{-1}] or illuminance [lx] and luminance [cd m^{-2}] for a long time. Recently, some applications require spectral irradiance [W m^{-2} nm^{-1}] and spectral radiance [W m^{-2} sr^{-1} nm^{-1}], e.g. architectural lighting design considering color rendering property (ISO 8995-1, 2002; Yoshida and Uetani, 2013), investigation of circadian rhythm (Brainard et al., 2001), photosynthesis analyses of vegetation (Gates et al., 1965) and evaluations of various photovoltaic cells (Field, 1997).

There are well known spectral models of direct and diffuse solar irradiance (Bird and Riordan, 1986; Gueymard, 1995), and spectroradiometer products are available to measure global, diffuse and direct solar spectral irradiance [W m^{-2} nm^{-1}]. However a few methods to measure the all sky distribution of spectral radiance [W m^{-2} sr^{-1} nm^{-1}] are developed (López-Álvarez, 2008; Roman, 2012) using large-scaled instruments which are not portable for field measurements in various climates. Another disadvantage of these instruments is the device dependent scheme in which the spectral calibration might be required to build other instruments.

The purpose of the research is to develop a practical method to measure the spectral radiance of all sky elements using a general purpose digital camera and a circular fisheye lens. The method is composed of two techniques: (a) Measurement of the all sky distribution of the absolute values of CIE 1931 tristimulus values X, Y[cd m^{-2}] and Z; (b) Estimation of the spectral radiance [W m^{-2} sr^{-1} nm^{-1}] of a sky element using principal component analysis from the XYZ values. Each technique is useful itself: (a) all sky distributions of XYZ are utilized as sky luminance [cd m^{-2}] and colorimetric values such as correlated color temperature [K]; (b) XYZ values of a sky element measured by conventional telescopic colorimeters are able to estimate spectral radiance. The accuracy of the method is experimentally validated by comparing with the spectral radiance of sky elements simultaneously measured by the spectroradiometer.

Selection and/or peer review under responsibility of EuroSun2014 Scientific Committee
doi:10.18086/eurosun.2014.08.13 Available at http://proceedings.ises.org

2. Colorimetric calibration of the digital camera with fisheye lens in consideration of correlated color temperature

The Video Colorimetry method (Uetani, 2001) colorimetrically calibrates a digital camera with a lens using a colorimeter, a xenon lamp, and color samples in a dark room. In the actual measurements, the colorimetric calibration function convert the RGB signal values (from 0 to 2^Q-1) of each pixel to the absolute values of CIE 1931 tristimulus values XYZ pixel by pixel, where Q is the bit depth of the camera and 'absolute' means that Y has the unit [cd m^{-2}]. The colorimetric calibration functions of each combination of a digital camera and a lens should be derived because even the same products have individual characteristics differences.

2.1 Basic equations

The Video Colorimetry method is modified (Yatsuzuka and Uetani, 2013) by introducing AdobeRGB color space (ADOBE, 2005). The color space of the digital camera must be set as 'AdobeRGB'. The RGB signal values of a pixel on the Q bit RGB color image (R'_{vQ} G'_{vQ}, B'_{vQ}) are read by appropriate image processing softwares and normalized to component values (R'_v, G'_v, B'_v) by equation (1).

$$\begin{cases} R'_v = R'_{vQ}/(2^Q-1) \\ G'_v = G'_{vQ}/(2^Q-1) \\ B'_v = B'_{vQ}/(2^Q-1) \end{cases} \quad (1)$$

The absolute values of CIE 1931 tristimulus values (X_s, Y_s, Z_s) measured by a colorimeter or spectroradiometer are converted to the tristimulus values (R_s, G_s, B_s) by equation (2), then transferred to the component values (R'_s, G'_s, B'_s) by equation (3).

$$\begin{bmatrix} R_s \\ G_s \\ B_s \end{bmatrix} = \begin{bmatrix} 2.04159 & -0.56501 & -0.34473 \\ -0.96924 & 1.87597 & 0.04156 \\ 0.01344 & -0.11836 & 1.01517 \end{bmatrix} \begin{bmatrix} X_s \\ Y_s \\ Z_s \end{bmatrix} \quad (2)$$

$$\begin{cases} R'_s = R_s^{1/2.19921875} \\ G'_s = G_s^{1/2.19921875} \\ B'_s = B_s^{1/2.19921875} \end{cases} \quad (3)$$

By the regression analysis between the component values (R'_s, G'_s, B'_s) and the normalized component values (R'_v, G'_v, B'_v), the colorimetric calibration functions (f_r, f_g, f_b) are derived as equation (4).

$$\begin{cases} R'_s = f_r(R'_v) \\ G'_s = f_g(G'_v) \\ B'_s = f_b(B'_v) \end{cases} \quad (4)$$

In the actual measurement, the RGB signal values of a pixel on the captured image (R'_{vQ} G'_{vQ}, B'_{vQ}) are transferred to the normalized component values (R'_v, G'_v, B'_v) by equation (1), then to the component values (R'_{vs}, G'_{vs}, B'_{vs}) by equation (4). These values are transferred to the tristimulus values (R_{vs}, G_{vs}, B_{vs}) by equation (5), then converted to the absolute tristimulus values (X_{vs}, Y_{vs}, Z_{vs}) by equation (6) where the value Y_{vs} has the unit [cd m^{-2}].

$$\begin{cases} R_{vs} = R'_{vs}{}^{2.19921875} \\ G_{vs} = G'_{vs}{}^{2.19921875} \\ B_{vs} = B'_{vs}{}^{2.19921875} \end{cases} \quad (5)$$

$$\begin{bmatrix} X_{vs} \\ Y_{vs} \\ Z_{vs} \end{bmatrix} = \begin{bmatrix} 0.57667 & 0.18556 & 0.18823 \\ 0.29734 & 0.62736 & 0.07529 \\ 0.02703 & 0.07069 & 0.99134 \end{bmatrix} \begin{bmatrix} R_{vs} \\ G_{vs} \\ B_{vs} \end{bmatrix} \quad (6)$$

2.2 Experiment

In the previous study (Yatsuzuka and Uetani, 2013), achromatic color samples (Macbeth ColorChecker, No.19-24) are used and found slightly lower accuracy for higher correlated color temperature sky. In this paper, 21 pieces of chromatic color samples (Color Atlas 5510 Color Guide) close to sky color are added.

In the dark room, as shown in Fig.1, a color sample is illuminated by a xenon lamp (USHIO Optical Modulex SX-UI501XQ) with ND filters (BK7). The maximum illuminance on the color sample is approximately 400,000 lx without ND filter. The transmittance of the ND filters are 1 (without ND filter), 0.1, 0.05, 0.005 and 0.001. The digital camera (Nikon, D300s: 14bit NEF, White balance; Cloudy, ISO; 200, Shutter speed; 1/250, F stop; 22, Color space; AdobeRGB) and the fisheye lens (Nikon, Fisheye Converter FC-E8) are connected by the wide lens (Nikon, AF Nikkor 20mm f/2.8D). The luminance range of the spectroradiometer (Photo Research, PR650, Field of view (FOV): 1°) is from 3.4 to 34,000 cd m^{-1}, and the maximum luminance is expanded with the ND filter (Photo Research, ND-2) to 3,400,000 cd m^{-1}. The spectroradiometer is raised up keeping the reflection angle 45° to avoid the interruption by the digital camera.

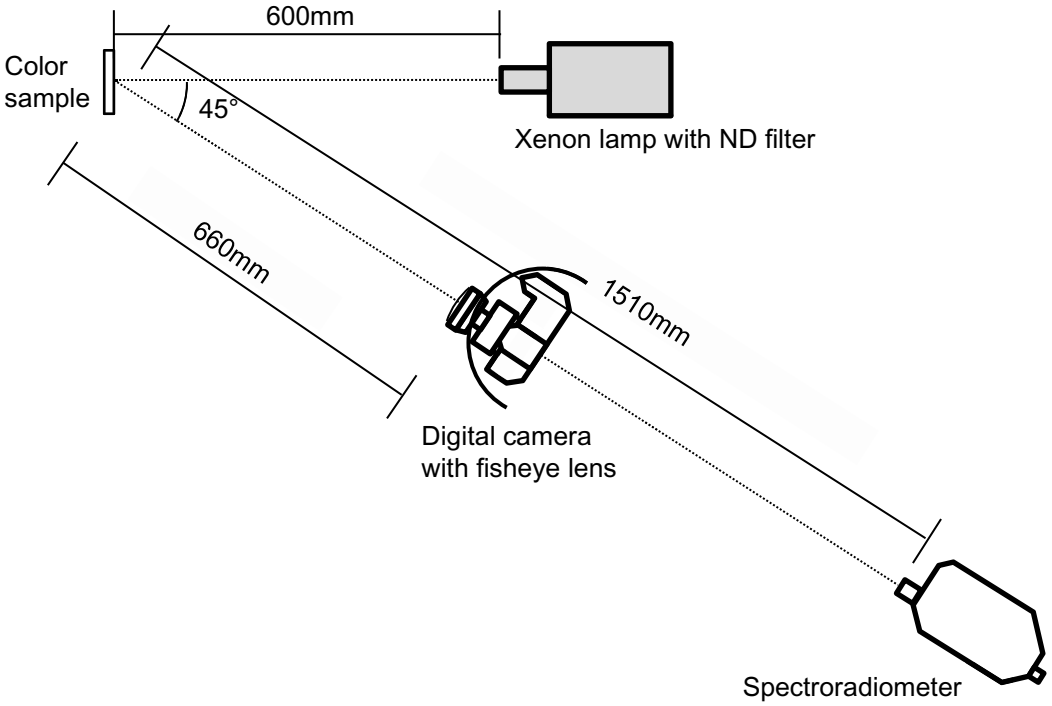

Fig. 1: Layout of the instruments

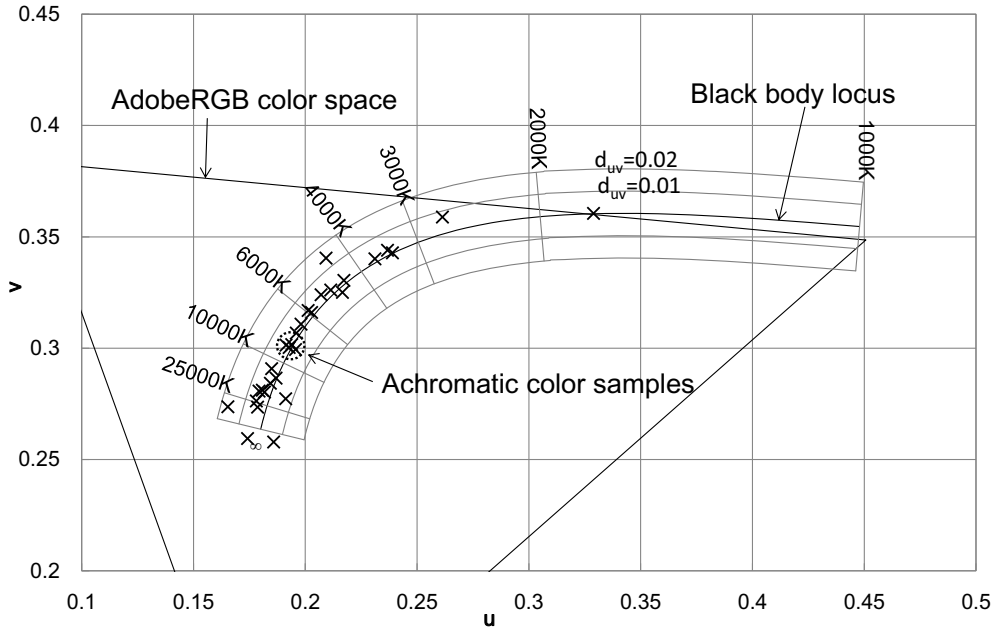

Fig. 2: 1960uv chromaticity coordinates of color samples measured by the spectroradiometer

Fig. 2 shows that the chromaticity coordinates of the reflected light are distributed along the black body locus

and the range of correlated color temperature is wide from 2000K to infinity. The data are divided into three groups (4000K<, 4000-10000K, 10000K≥) by correlated color temperature.

Because the fisheye lens (Nikon, Fisheye Converter FC-E8) is optically designed for the old compact digital cameras (Nikon, COOLPIX series), the irregular combination with the digital still camera and the wide lens causes the vignetting shown in Fig. 3. As the preprocessing to the colorimetric calibration, the vignetting correction functions are applied to each image. At the same time, each equidistance image is converted to equisolid angle image.

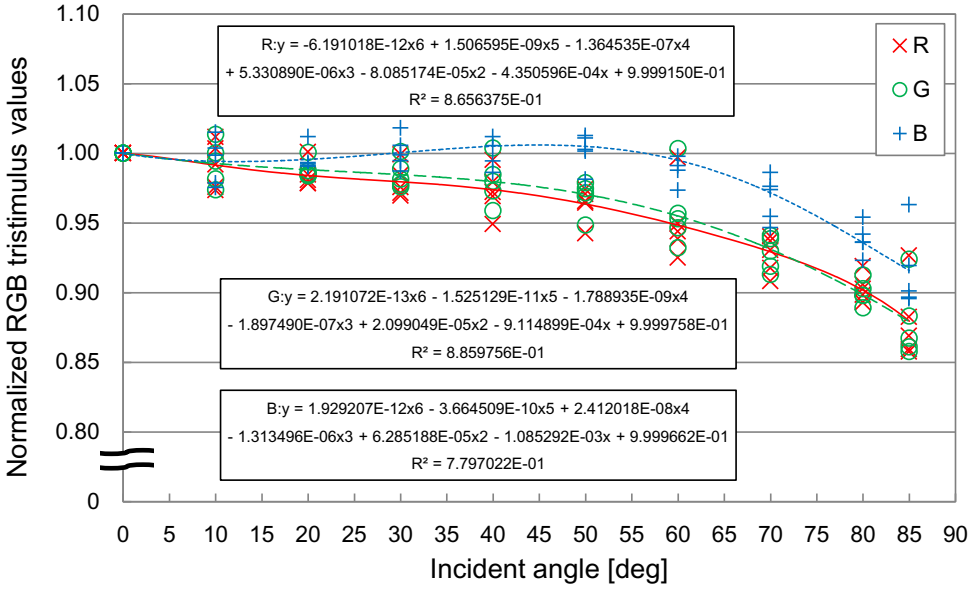

Fig. 3: Vignetting correction functions of Tristimulus values RGB

The regression analyses are performed to the three groups by polynomial equations (7). Tab. 1 shows the results as the coefficients of the colorimetric calibration functions and high R^2. Fig. 4 demonstrates the good agreement of the colorimetric calibration functions and measured data by dividing into three groups.

$$\begin{cases} f_r(R'_v) = a_{6,r}R'^{6}_v + a_{5,r}R'^{5}_v + a_{4,r}R'^{4}_v + a_{3,r}R'^{3}_v + a_{2,r}R'^{2}_v + a_{1,r}R'_v + a_{0,r} \\ f_g(G'_v) = a_{6,g}G'^{6}_v + a_{5,g}G'^{5}_v + a_{4,g}G'^{4}_v + a_{3,g}G'^{3}_v + a_{2,g}G'^{2}_v + a_{1,g}G'_v + a_{0,g} \\ f_g(B'_v) = a_{6,b}B'^{6}_v + a_{5,b}B'^{5}_v + a_{4,b}B'^{4}_v + a_{3,b}B'^{3}_v + a_{2,b}B'^{2}_v + a_{1,b}B'_v + a_{0,b} \end{cases} \quad (7)$$

Tab. 1: Coefficients of the colorimetric calibration functions and R^2 as the results of the regression analyses

		a_6	a_5	a_4	a_3	a_2	a_1	a_0	R^2
4000K <	R	-	8.984E+2	-2.511E+3	2.592E+3	-1.110E+3	2.880E+2	8.276E+0	0.999
	G	-	4.422E+2	-1.475E+3	1.680E+3	-7.539E+2	2.429E+2	7.010E+0	0.999
	B	-	-	-3.839E+3	3.710E+3	-1.212E+3	2.940E+2	3.042E+0	0.994
4000-10000K	R	-4.418E+2	1.939E+3	-3.148E+3	2.520E+3	-9.660E+2	2.645E+2	7.194E+0	0.999
	G	-1.145E+3	3.520E+3	-4.437E+3	2.964E+3	-1.012E+3	2.593E+2	6.798E+0	0.999
	B	-1.560E+3	4.929E+3	-6.121E+3	3.847E+3	-1.213E+3	2.804E+2	6.201E+0	0.998
10000K >=	R	1.611E+3	-1.151E+3	-1.900E+3	2.498E+3	-9.956E+2	2.615E+2	5.235E+0	0.999
	G	1.750E+3	-2.838E+3	6.722E+2	1.099E+3	-6.968E+2	2.327E+2	6.478E+0	0.999
	B	-	2.317E+2	-9.937E+2	1.400E+3	-7.385E+2	2.410E+2	9.427E+0	0.999

Fig. 5 shows the scatter diagrams of the estimated tristimulus values XYZ by the colorimetric calibration functions using fisheye digital camera images and the measured XYZ by the spectroradiometer. The values of the statistical criteria (%RMSE, %MBE) show that the Video Colorimetry method accurately measures the absolute tristimulus values XYZ. The colorimetric calibration functions cover the luminance from 70 to 50,000 cd m^{-2} as shown in Tab. 2. This range is able to be raised or lowered by changing the shutter speed.

Tab. 2: Range of XYZ values covered by the colorimetric calibration functions for the shutter speed: 1/250

	X	Y [cd m^{-2}]	Z
max	48733	49369	61189
min	65	68	58

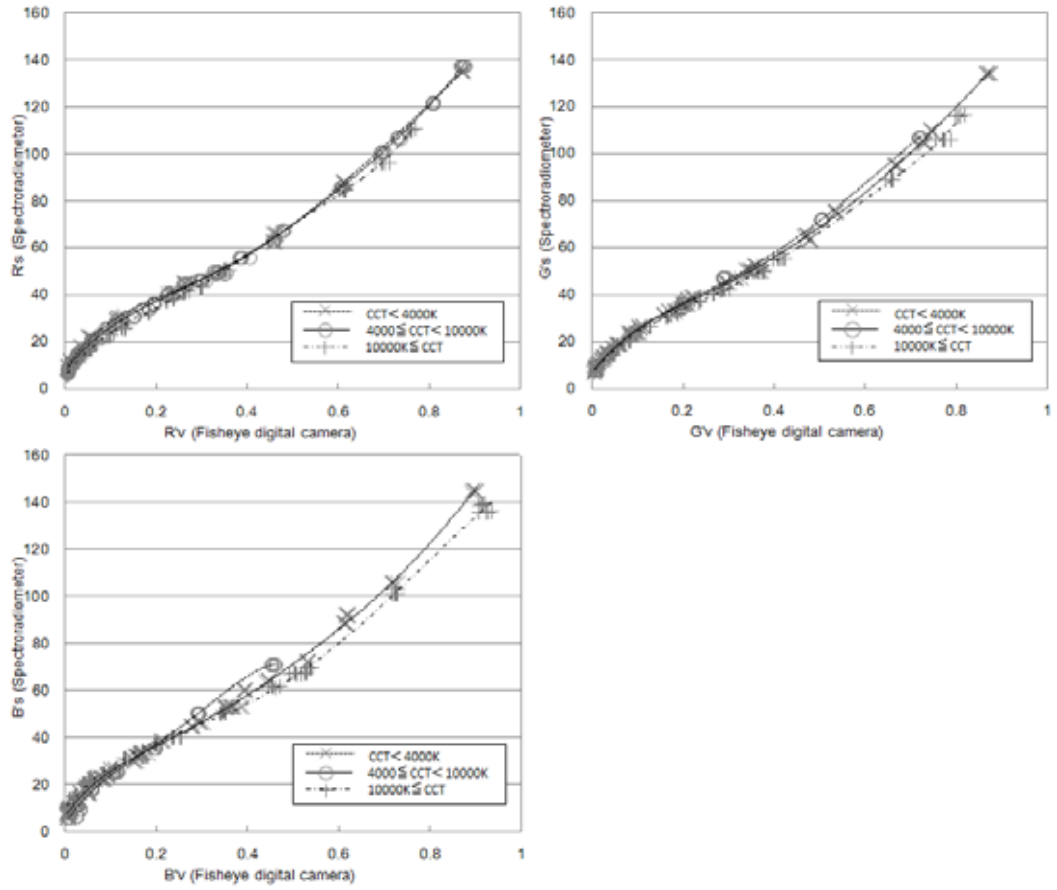

Fig. 4: Colorimetric calibration functions and measured data

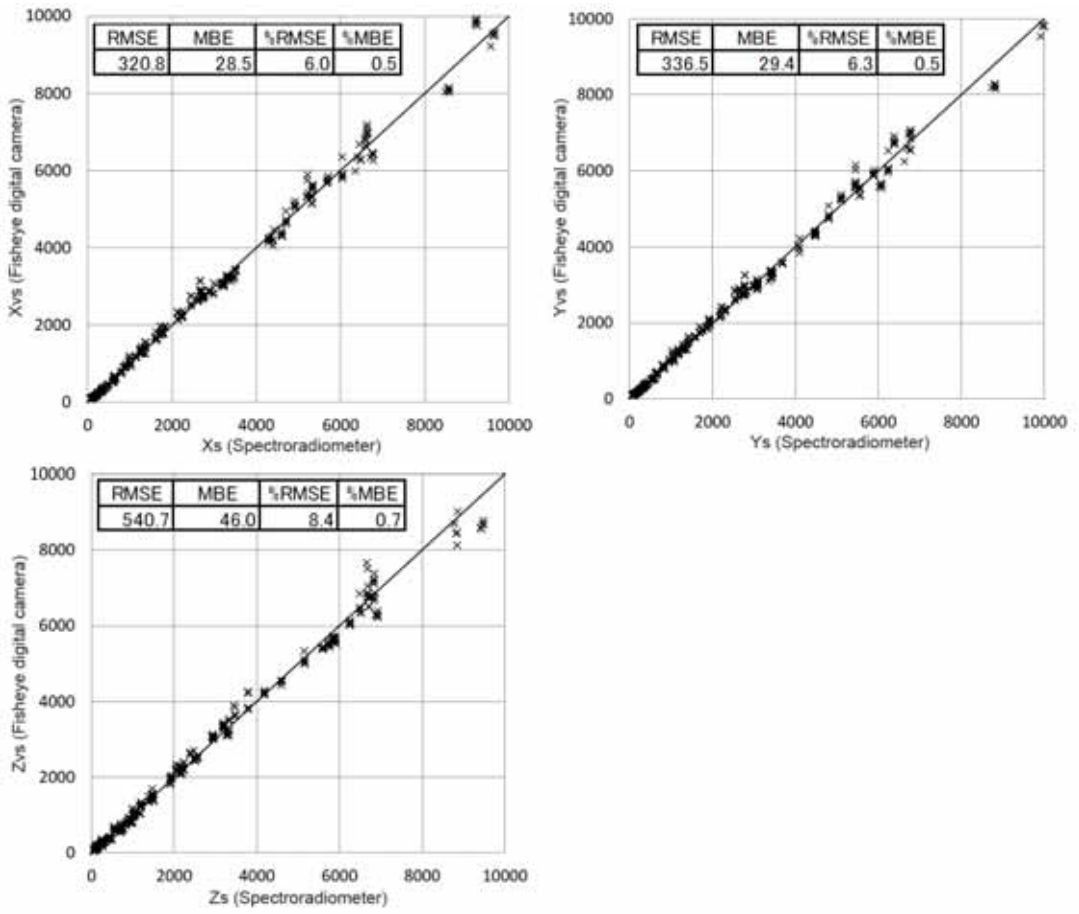

Fig. 5: Scatter diagrams of the estimated XYZ by fisheye digital camera and the measured XYZ by spectroradiometer

3. Estimation of the spectral radiance of a sky element using principal component analysis from the absolute XYZ values

The XYZ tristimulus values of a sky element are transferred into the spectral radiance using the eigenvectors obtained by principal component analysis (PCA) of the spectral radiance of sky elements measured by a spectroradiometer.

The original method (Yatsuzuka and Uetani, 2013) used the three eigenvectors obtained by principal component analysis of the spectral radiance of sky elements measured by a spectroradiometer. The absolute XYZ tristimulus values of a sky element directly reconstructed the the spectral radiance [W m^{-2} sr^{-1} nm^{-1}]. It was straightforward but less accurate for the sky of high correlated color temperature. In the further investigation, the third proportion of variance was considerably lower than first and second coefficients.

The improved method (Yatsuzuka and Uetani, 2014) transfers the absolute XYZ tristimulus values of a sky element into the CIE 1931 chromaticity coordinates xy, and the relative spectral power distribution is calculated using the two eigenvectors (Judd et al., 1964). Then it is transferred to the absolute spectral radiance [W m^{-2} sr^{-1} nm^{-1}] by the one of the absolute tristimulus values (luminance) Y [cd m^{-2}].

3.1 Basic equations

The spectral radiance $L_{meas}(\lambda_i)$ [W m^{-2} sr^{-1} nm^{-1}] of various sky elements measured by a spectroradiometer are normalized to 1 at 555nm as the relative spectral power distribution $S_{meas}(\lambda_i)$ by equation (8), then the eigenvectors $A_k(\lambda_i)$ ($k = 1,2$) are obtained by principal component analysis.

$$S_{meas}(\lambda_i) = \frac{L_{meas}(\lambda_i)}{L_{meas}(555)} \tag{8}$$

The chromaticity coordinates (x, y) are calculated using the tristimulus values (X, Y, Z) of a sky element. The scalar multiples M_1 and M_2 are calculated by equation (9), and the relative spectral power distribution $S(\lambda_i)$ is constructed by equation (10) (Judd et al., 1964).

$$\begin{cases} M_1 = \dfrac{X_{r,2}\bar{Y}_r - \bar{X}_r Y_{r,2} + \left(\bar{W}\,Y_{r,2} - \bar{Y}_r W_2\right)x + \left(\bar{X}_r W_2 - \bar{W}\,X_{r,2}\right)y}{X_{r,1}Y_{r,2} - Y_{r,1}X_{r,2} + \left(Y_{r,1}W_2 - W_1 Y_{r,2}\right)x + \left(W_1 X_{r,2} - X_{r,1}W_2\right)y} \\ M_2 = \dfrac{Y_{r,1}\bar{X}_r - X_{r,1}\bar{Y}_r + \left(W_1\bar{Y}_r - Y_{r,1}\bar{W}\right)x + \left(X_{r,1}\bar{W} - W_1\bar{X}_r\right)y}{X_{r,1}Y_{r,2} - Y_{r,1}X_{r,2} + \left(Y_{r,1}W_2 - W_1 Y_{r,2}\right)x + \left(W_1 X_{r,2} - X_{r,1}W_2\right)y} \end{cases} \tag{9}$$

$$S(\lambda_i) = \bar{S}_{meas}(\lambda_i) + \sum_{k=1}^{2} M_k A_k(\lambda_i) \tag{10}$$

where, $\bar{S}_{meas}(\lambda_i)$ is the mean of all $S_{meas}(\lambda_i)$. ($X_{r,1}$, $Y_{r,1}$, $Z_{r,1}$), ($X_{r,2}$, $Y_{r,2}$, $Z_{r,2}$), ($\bar{X}_r$, $\bar{Y}_r$, $\bar{Z}_r$), $\bar{W}$ and (W_1, W_2) are calculated by equations from (11) to (14).

$$\begin{cases} X_{r,k} = \sum_{i=1}^{m} A_k(\lambda_i)\bar{x}(\lambda_i)\Delta\lambda \\ Y_{r,k} = \sum_{i=1}^{m} A_k(\lambda_i)\bar{y}(\lambda_i)\Delta\lambda \\ Z_{r,k} = \sum_{i=1}^{m} A_k(\lambda_i)\bar{z}(\lambda_i)\Delta\lambda \end{cases} \quad (k = 1, 2) \tag{11}$$

$$\begin{cases} \bar{X}_r = \sum_{i=1}^{m} \bar{S}_{meas}(\lambda_i)\bar{x}(\lambda_i)\Delta\lambda \\ \bar{Y}_r = \sum_{i=1}^{m} \bar{S}_{meas}(\lambda_i)\bar{y}(\lambda_i)\Delta\lambda \\ \bar{Z}_r = \sum_{i=1}^{m} \bar{S}_{meas}(\lambda_i)\bar{z}(\lambda_i)\Delta\lambda \end{cases} \tag{12}$$

$$\bar{W} = \bar{X}_r + \bar{Y}_r + \bar{Z}_r \tag{13}$$

$$W_k = X_{r,k} + Y_{r,k} + Z_{r,k} \quad (k = 1, 2) \tag{14}$$

The coefficient r is calculated using the luminance Y [cd m^{-2}] and the relative spectral power distribution $S(\lambda_i)$ by equation (15), and $S(\lambda_i)$ is converted to the spectral radiance $L(\lambda_i)$ [W m^{-2} sr^{-1} nm^{-1}] by equation (16).

$$r = Y \Big/ \mathrm{K} \sum_{380}^{780} S(\lambda_i)\bar{y}(\lambda_i)\Delta\lambda \tag{15}$$

$$L(\lambda_i) = r\,S(\lambda_i) \tag{16}$$

As the statistical criteria %RMSE, %MBE and GFC are used. GFC (goodness-fitting coefficient) is calculated by equation (17) and the spectral accuracy is evaluated as GFC $\geq$ 0.995:*colorimetrically accurate*, GFC $\geq$ 0.999:*good*, GFC $\geq$ 0.9999:*excellent* (Romero, 1997).

$$GFC = \frac{\left|\sum_{i=1}^{m} L_{meas}(\lambda_i) L(\lambda_i)\right|}{\sqrt{\sum_{i=1}^{m} L_{meas}(\lambda_i)^2} \sqrt{\sum_{i=1}^{m} L(\lambda_i)^2}} \quad (17)$$

3.2 Experiment

In the first stage, the spectroradiometer (Photo Research, PR650, FOV 1°) are mounted on the angle scaled platform as shown in Fig. 6(a). We manually scanned the whole sky with the angular resolution of 0.5°, and measured 1324 spectral radiance data on three days between 2011/12/7 and 2013/2/28. In the second stage, the spectroradiometer and an USB camera for monitoring are mounted on the automatic pan-tilt unit (FLIR, PTU-48E) as shown in Fig. 6(b). A LabVIEW program automatically scanned the whole sky in the CIE IDMP 145 directions (CIE 108, 1994) with the precise angular resolution (Pan:0.006°, Tilt:0.003°), and measured 1388 spectral radiance data on three days between 2013/12/14 and 2014/1/22.

Fig. 6: Spectroradiometer on the angle scaled platform (a: left) and automatic pan-tilt unit controlled by a PC (b: right)

Fig. 7 shows the eigenvectors and mean derived from 2712 measured relative spectral power distribution data. The proportion of variance and cumulative contribution shown in Tab. 3 explain that the first and second eigenvectors are necessary and sufficient. Tab. 4 shows the good accuracy of 2712 constructed and measured spectral radiance [W m^{-2} sr^{-1} nm^{-1}] by the averages of %RMSE, %MBE and GFC.

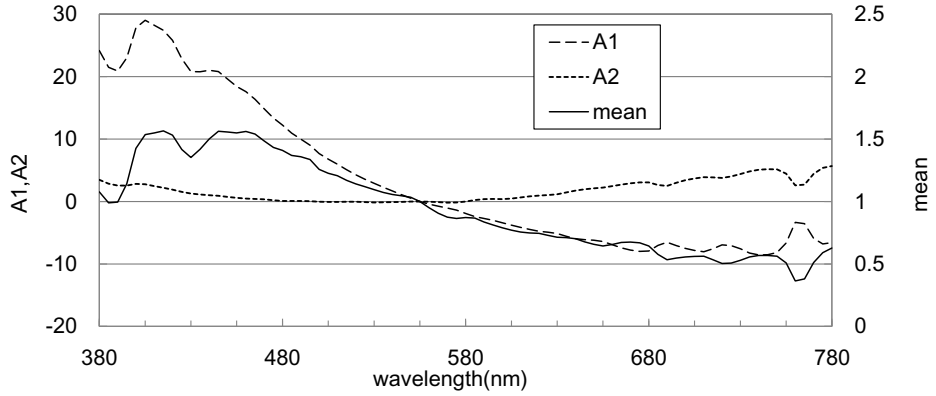

Fig. 7: Eigenvectors and mean of the measured relative spectral power distribution

Tab. 3: Proportion of variance and Cumulative contribution

	A1	A2	A3
Proportion of Variance	0.9486	0.0376	0.0097
Cumulative contribution	0.9486	0.9862	0.9960

Tab. 4: The averages of statistical criteria

Accuracy (n=2712)		
%RMSE	%MBE	GFC
4.7	−0.1	0.99851 (c)

(c): colorimetrically accurate

4. Measuremet of the all sky spectral radiance distribution using the fisheye digital camera and the validation

4.1 Long-term measurement

The fisheye digital camera is installed at the CIE IDMP station on the rooftop highest in the campus and the

neighborhood. The camera is covered by a stainless bowl against rain and solar radiation for the long-term measurement as shown in Fig. 8. The camera is connected to a PC for the interval capturing. The regular capturing every 15 minute had been performed from 2013/2/25 to 2013/6/26 and from 2013/11/18 to 2014/2/15, from 2 hours before sunrise and 2 hours after sunset. In the period, approximately 9000 images were captured. Fig. 9 is an example image captured at 12:00 JST on 2014/1/10.

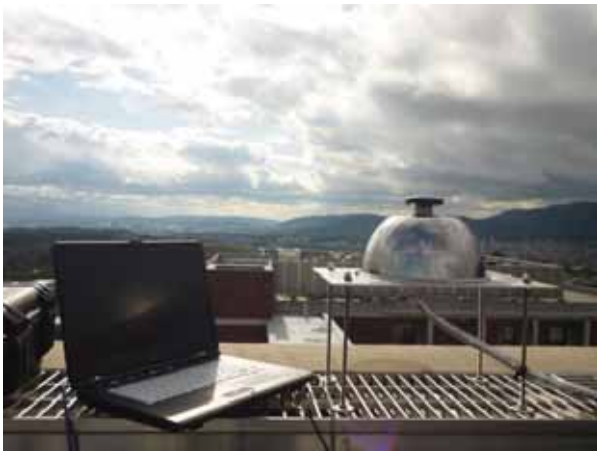

Fig. 8: Installed fisheye camera for long-term measurement

Fig. 9: All sky image captured at 12:00 on 2014/1/10

4.2 Validation

The preliminary validation using the fisheye camera shown in Fig. 8 and the spectroradiometer mounted on the automatic pan-tilt unit shown in Fig. 6(b) were performed. The time difference caused errors because the winds drove out the clouds quickly from the small FOV(1°) of the spectroradiometer.

The spectroradiometer, the USB monitoring camera and the fisheye camera are mounted on the automatic pan-tilt unit as shown in Fig. 10. The spectroradiometer and the pan-tilt unit are operated synchronously with the interval capturing fisheye camera.

Fig. 10: Validation instruments on the pan-tilt unit

Tab. 5: The statistical criteria (274 data)

	Average	Max	Min	SD
%RMSE	10.0	36.0	2.3	4.5
%MBE	2.3	20.2	-35.3	6.3
GFC	0.99643 (c)	0.99982 (g)	0.98562 (-)	0.00271

(g): good, (c):colorimetrically accurate

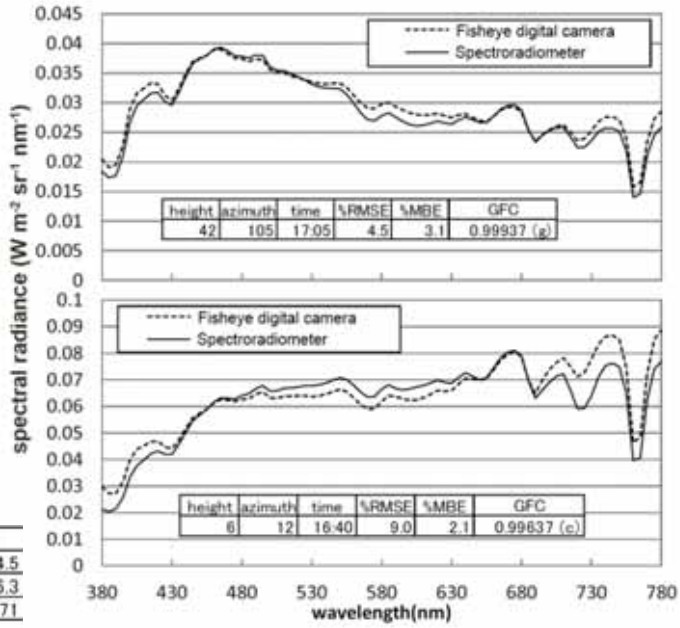

Fig. 12: Reconstructed spectral radiance

The system scanned the whole sky and measured 274 data on 2014/2/16 and 2/17. Fig. 11 shows the scatter diagrams of the estimated tristimulus values XYZ by the fisheye digital camera images and the measured XYZ by the spectroradiometer. The values of the statistical criteria show that the Video Colorimetry method in the unstable field measurements is as accurate as in the dark room experiments. Tab. 5 shows the *colorimetrically accurate* results of 274 constructed and measured spectral radiance [W m^{-2} sr^{-1} nm^{-1}]. Fig. 12 shows the examples of reconstructed spectral radiance, (c): *colorimetrically accurate* and (g): *good* in which the difference is a little.

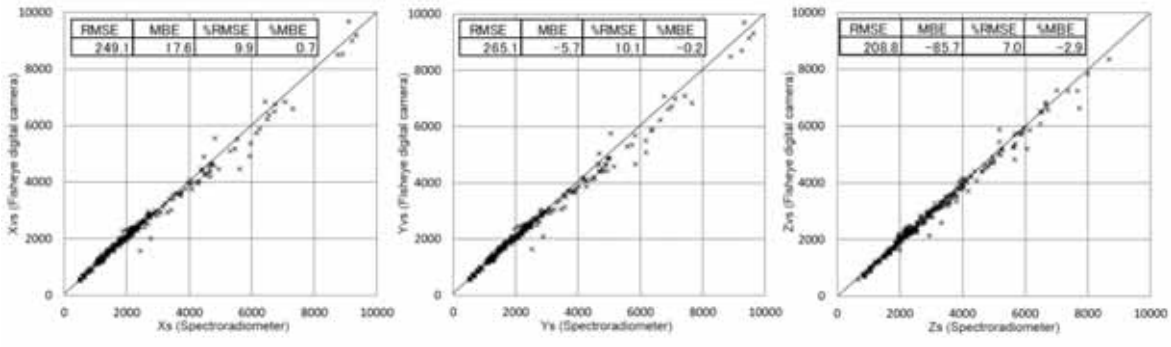

Fig. 11: Scatter diagrams of the estimated XYZ by fisheye digital camera and the measured XYZ by spectroradiometer

5. Prototype of the all sky spectral radiance distribution database

While the long-term measurement was performed from 2013/2/25 to 2014/2/15, the CIE IDMP observation was in operation. Approximately 9000 images are captured, converted to equisolid angle images, and transferred to the absolute XYZ values pixel by pixel. Each 180° circular image has 4 million pixels. For saving the storage and quick response, the sky is divided by the patterns of FOV =1°, 3°, 5° and 11° as shown in Fig. 12. The pattern of FOV =11° is the same as CIE IDMP recommendation (CIE 108, 1994). For each FOV pattern, the average values of the absolute XYZ and spectral radiance values are calculated and stored.

Because the interval of sky images is 15 minutes, the IDMP observed data are stored as 15 minutes average values which are arranged as the searching sheet shown in Fig. 13. The hyperlink in the searching sheet opens the display sheet in which the altitude and azimuth angles of the sky element are entered and spectral radiance graphs of FOV =1°, 3°, 5° and 11° are drawn as shown in Fig. 14.

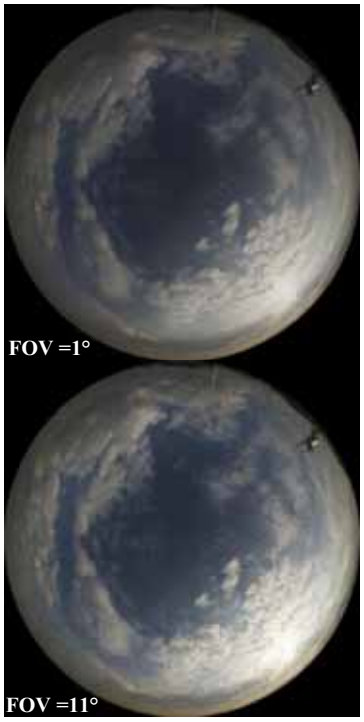

Fig. 12: The sky patterns

Tab. 13: IDMP observed data searching sheet

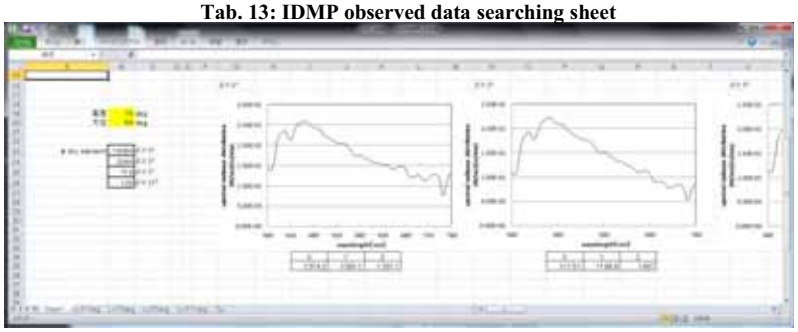

Tab. 14: Spectral radiance graphs of display sheet

6. Conclusions

The Video Colorimetry method expands the functions of a general purpose digital camera with a circular fisheye lens to accurately measure the absolute values of the CIE 1931 tristimulus values X, Y[cd m^{-2}], Z pixel by pixel of all sky images. Using principal component analysis, the spectral radiance [W m^{-2} sr^{-1} nm^{-1}] of each pixel is estimated by the absolute XYZ values. The combination of the two techniques enables the

fisheye camera to measure the all sky spectral radiance distribution. The experimental validation evaluated the new method as *colorimetrically accurate*. In the long-term measurement performed for one year, approximately 9000 sky images were captured every 15 minute while the CIE IDMP observation was in operation. The sky images are processed into a prototype of the all sky spectral radiance distribution database in which the IDMP data are arranged to search the all sky spectral radiance distribution.

The author wishes to acknowledge Mr. Hideki Yatsuzuka for his earnest assistance. This research was supported by JSPS KAKENHI Grant Number 25630237.

7. References

ADOBE SYSTEMS, 2005. Adobe RGB (1998) Color Image Encoding Version 2005-05.

Richard E. Bird, Carol Riordan, 1986. Simple Solar Spectral Model for Direct and Diffuse Irradiance on Horizontal and Tilted Planes at the Earth's Surface for Cloudless Atmospheres. J. Climate Appl. Meteor. 25, 87–97.

George C. Brainard et al., 2001. Action Spectrum for Melatonin Regulation in Humans: Evidence for a Novel Circadian Photoreceptor, Journal of Neuroscience, 21, 16, 6405–6412.

CIE 108, 1994. Guide to Recommended Practice of Daylight Measurement, Vienna.

H. Field, 1997. Solar Cell Spectral Response Measurement Errors Related to Spectral Band Width and Chopped Light Waveform, http://www.nrel.gov/docs/legosti/fy97/22969.pdf (accessed Dec. 1, 2013)

David M. Gates et al., 1965. Spectral Properties of Plants, Applied Optics, 4, 1, 11-20.

Christian Gueymard, 1995. SMARTS2, A Simple Model for the Atmospheric Radiative Transfer of Sunshine: Algorithms and performance assessment, FSEC-PF-270-95, Florida Solar Energy Center.

ISO 8995-1, 2002. (CIE S 008/E:2001), Lighting of indoor work places -- Part 1: Indoor

DEANE B. JUDD, DAVID L. MACADAM, GUNTER WYSZECKI, H. W. BUDDE, H. R. CONDIT, S. T. HENDERSON, J. L. SIMONDS, 1964. Spectral Distribution of Typical Daylight as a Function of Correlated Color Temperature, JOSA, 54, 8, 1031-1040.

Miguel A. López-Álvarez, Javier Hernández-Andrés, Javier Romero, F. J. Olmo, A. Cazorla, L. Alados-Arboledas, 2008. Using a trichromatic CCD camera for spectral skylight estimation, Applied Optics 47, 34, 31-38.

R. Román, M. Antón, A. Cazorla, A. de Miguel, F. J. Olmo, J. Bilbao, and L. Alados-Arboledas, 2012, Calibration of an all-sky camera for obtaining sky radiance at three wavelengths, Atmos. Meas. Tech. 5, 2013–2024.

Javier Romero, Antonio Garcı´a-Beltra´n, Javier Herna´ndez-Andre´s, 1997. Linear bases for representation of natural and artificial illuminants, JOSA, 14, 5, 1007-1014.

Yoshiaki Uetani, 2001. Measurement of CIE Tristimulus Values XYZ by Color Video Images - Development of Video Colorimetry -, Journal of Architecture, Planning and Environmental Engineering (Transactions of AIJ), 543, 25-31.

Hideki Yatsuzuka, Yoshiaki Uetani, 2013. Measurement of the All Sky Spectral Radiance Distribution using a Digital Camera with a Fisheye Lens, Journal of Environmental Engineering (Transactions of AIJ), 78, 690, 623-629 (in Japanese).

Hideki Yatsuzuka, Yoshiaki Uetani, 2014. Estimation of the Spectral Radiance of a Sky Element using Pricipal Component Analysis, Journal of Environmental Engineering (Transactions of AIJ), 79, 697, 227-232 (in Japanese).

Gorou Yoshida, Yoshiaki Uetani, 2013. Evaluation of Color Rendering Properties of Daylighting with Artificial Lighting by Calculating Spectral Interreflection, Journal of Environmental Engineering (Transactions of AIJ), 78, 691, 697-702 (in Japanese).